PLOS COMPUTATIONAL BIOLOGY

RESEARCH ARTICLE

Mathematical modeling identifies optimum lapatinib dosing schedules for the treatment of glioblastoma patients

Shayna Stein[1,2,3,4], Rui Zhao[1,2], Hiroshi Haeno[5], Igor Vivanco[6]*, Franziska Michor[1,2,3,4,7]*

1 Department of Biostatistics, Harvard T. H. Chan School of Public Health, Boston, Massasschusetts, United States of America, **2** Department of Biostatistics and Computational Biology, Dana-Farber Cancer Institute, Boston, Massachusetts, United States of America, **3** Department of Stem Cell and Regenerative Biology, Harvard University, Cambridge, Massachusetts, United States of America, **4** The Broad Institute of Harvard and MIT, Cambridge, Massachusetts, United States of America, **5** Department of Biology, Kyushu University, Fukuoka, Japan, **6** Division of Cancer Therapeutics, The Institute of Cancer Research, London, United Kingdom, **7** Center for Cancer Evolution, Dana-Farber Cancer Institute, Boston, Massachusetts, United States of America

* igor.vivanco@icr.ac.uk (IV); michor@jimmy.harvard.edu (FM)

Citation: Stein S, Zhao R, Haeno H, Vivanco I, Michor F (2018) Mathematical modeling identifies optimum lapatinib dosing schedules for the treatment of glioblastoma patients. PLoS Comput Biol 14(1): e1005924. https://doi.org/10.1371/journal.pcbi.1005924

Editor: Alexander R.A. Anderson, H. Lee Moffitt Cancer Center and Research Institute, UNITED STATES

Received: January 22, 2017

Accepted: December 12, 2017

Published: January 2, 2018

Data Availability Statement: All data are contained in the paper.

Funding: We would like to acknowledge support from the Dana-Farber Cancer Institute Physical Sciences-Oncology Center (U54 CA193461, to FM) and from the NIH/NIGMS T32 GM074897 training grant (to SS). The funders had no role in study design, data collection and analysis, decision to publish, or preparation of the manuscript.

Abstract

Human primary glioblastomas (GBM) often harbor mutations within the epidermal growth factor receptor (EGFR). Treatment of EGFR-mutant GBM cell lines with the EGFR/HER2 tyrosine kinase inhibitor lapatinib can effectively induce cell death in these models. However, EGFR inhibitors have shown little efficacy in the clinic, partly because of inappropriate dosing. Here, we developed a computational approach to model the *in vitro* cellular dynamics of the EGFR-mutant cell line SF268 in response to different lapatinib concentrations and dosing schedules. We then used this approach to identify an effective treatment strategy within the clinical toxicity limits of lapatinib, and developed a partial differential equation modeling approach to study the *in vivo* GBM treatment response by taking into account the heterogeneous and diffusive nature of the disease. Despite the inability of lapatinib to induce tumor regressions with a continuous daily schedule, our modeling approach consistently predicts that continuous dosing remains the best clinically feasible strategy for slowing down tumor growth and lowering overall tumor burden, compared to pulsatile schedules currently known to be tolerated, even when considering drug resistance, reduced lapatinib tumor concentrations due to the blood brain barrier, and the phenotypic switch from proliferative to migratory cell phenotypes that occurs in hypoxic microenvironments. Our mathematical modeling and statistical analysis platform provides a rational method for comparing treatment schedules in search for optimal dosing strategies for glioblastoma and other cancer types.

Author summary

In vivo inhibition of tumor expansion requires a sufficient amount of therapeutic agent to be present in the tumor tissue. A number of factors affect drug concentrations including

Competing interests: The authors have declared that no competing interests exist.

the maximum tolerated dose, pharmacokinetics and pharmacodynamics profiles. We present a computational modeling platform incorporating both in vitro data and published clinical trial data to investigate the efficacy of lapatinib as a function of different dosing schedules for inhibiting glioblastoma tumor cell growth. The goal of our method is to find the best dosing schedule balancing both toxicity and efficacy. Our modeling approach identifies continuous dosing as the best clinically feasible strategy for slowing down tumor growth even when taking into consideration intratumor heterogeneity, drug resistance and reduced lapatinib concentrations in the tumor due to the blood brain barrier.

Introduction

Glioblastoma is the most common and aggressive form of brain tumors in adults, characterized by short survival and poor treatment response [1]. Currently, the standard of care for glioblastoma patients includes surgery followed by radiotherapy and adjuvant chemotherapy with temozolomide [2]. However, the addition of chemotherapy only modestly prolongs survival (median 14.6 months) compared to radiation alone (median 12.1 months). Thus, there remains a pressing unmet medical need for more effective therapeutic agents. Unfortunately, since the introduction of temozolomide, no other compound has been able to significantly prolong patient survival in clinical trials. For orally administered drugs, most trials have only explored daily continuous dosing schedules (Table 1). However, there is increasing evidence that for some targeted agents, intermittent schedules can deliver equal or potentially even superior therapeutic benefit with less toxicity [3, 4].

In the last decade, several molecularly targeted agents that inhibit recurrently mutated proteins have been investigated as a therapeutic strategy in glioblastoma. These have included several inhibitors of the epidermal growth factor receptor (EFGR), which is mutationally activated in approximately 50% of adult GBMs. Lapatinib is a small molecule tyrosine kinase inhibitor of human epidermal receptor 2 (HER2) and EGFR, which currently has regulatory approval for the treatment of HER2-positive advanced or metastatic breast cancer [5]. Additional indications for lapatinib [6–14] including glioblastoma, are currently being explored [15, 16]. In GBM, clinical trials of lapatinib have failed to show efficacy using continuous dosing [15, 16]. Interestingly, a study that evaluated EGFR inhibition as a means to prime tumor vasculature for efficient delivery of chemotherapy showed that in glioblastoma patients, a 2-day pulse of high dose (5,250 mg/day) lapatinib given through twice daily dosing was well

Table 1. Dosing strategies for orally administrated drugs for GBM from published clinical trials.

Study	Treatment	Patients (N)	Dosing strategies
Rich et al. [77]	Gefinitib	53	500-1000mg daily
Prados et al. [78]	Erlotinib	83	100-500mg daily
Brown et al. [79]	Erlotinib	100	150mg daily
Reardon et al. [80]	Imatinib	33	500mg twice daily
Wen et al. [81]	Imatinib	55	600-800mg daily
Raymond et al. [82]	Imatinib	112	600mg daily—500mg twice daily
Reardon et al. [15]	Lapatinib	41	1000mg twice daily
Thiessen et al. [16]	Lapatinib	17	1000-1500mg twice daily
Chien et al. [17]	Lapatinib	25	1000-5250mg twice daily for two days in a 5-day cycle

https://doi.org/10.1371/journal.pcbi.1005924.t001

tolerated [17]. However, the question remains whether an altered dosing strategy might increase the efficacy of this agent. Due to ethical concerns of testing several dosing strategies in the absence of preclinical data suggesting their benefit, as well as to speed up discovery, mathematical modeling of treatment response can be used to identify predicted best administration schedules. Here, we explored continuous and pulsatile dosing strategies in an EGFR-mutant GBM cell line, and used mathematical and statistical modeling to determine optimal lapatinib dosing schedules for inhibiting tumor growth.

The use of mathematical models for treatment optimization is part of a growing effort to improve clinical trial design for cancer patients. Many models have been developed to investigate the relationship between toxicity and dose in an attempt to better characterize the toxicity profile of the therapeutic products under investigation. For instance, Huitema et al. reviewed several differential equation-based models of chemotherapy-induced myelosuppression, cardiovascular events and other ordinal adverse events [18]. Amantea et al. developed a model incorporating exposure, biomarkers, efficacy endpoints and adverse events in models describing the treatment response of patients with gastrointestinal stromal tumors [19]. Their analysis uncovered a correlation between adverse events and efficacy: drug-induced increases in diastolic blood pressure were positively associated with overall survival. Another study by Huitema et al. examined the effects of the anti-angiogenic drug E7080 and its drug-induced adverse events in an attempt to evaluate dosing regimens with regard to their reduction of adverse events and improvement of efficacy [20]. They found that proteinuria could be best described by a discrete-time Markov transition model. Similarly, Fuhr et al. constructed a continuous-time Markov model to investigate erlotinib-induced adverse events in non-small cell lung cancer patients; their simulation results provided support for the use of high-dose pulses as an alternative dosing strategy for addressing acquired resistance often found when using a low continuous dose [21]. In these examples, a delicate balance between toxicity and efficacy determines the most efficacious dose.

In addition to understanding toxicity profiles, mathematical models have also been used to model pre-clinical data from animal or in vitro systems in order to bypass the difficulty associated with directly observing tumor progression in humans. Translational models incorporating in vitro or animal data have also be developed to investigate the relationship between efficacy endpoints and exposure. Mould et al. provided a comprehensive review of how the use of mathematical models can aid early development of anti-cancer therapy, in particular for describing tumor volume as a function of drug exposure [22]. Most papers these authors discussed describe changing tumor volumes using differential equation models with two terms: net tumor growth in the absence of therapeutic candidates and a drug-induced shrinkage effect [23–27]. These models suggest that the best strategy for inhibiting tumor growth is to maximize the effect of drug exposure, which often corresponds to higher drug concentrations. However, given toxicity constraints, high drug concentrations usually cannot be achieved for long time periods. An alternative strategy is to administer drugs in pulsatile doses in order to circumvent the toxicity limit. A small trial using weekly pulsatile high-dose erlotinib showed promising results for controlling central nervous system metastases from epidermal growth factor receptor-mutant non-small cell lung cancer [28]. Crooke et al. also performed computational analyses comparing continuous and pulsatile dosing and found that pulsed therapy is more effective than continuous therapy [29]. A clinical trial [30] based on mathematical modeling and preclinical [31] experiments demonstrated that a combined low-dose continuous and high-dose pulsed erlotinib schedule was successful at preventing progression in patients with CNS metastases but did not show significantly delayed emergence of resistance due to the T790M EGFR mutation.

Here we present a computational modeling approach incorporating both toxicity data from phase I clinical trials and efficacy data from pre-clinical research to examine the effects of various lapatinib dosing schedules on tumor growth (Fig 1). The goal of our work is to determine the best dosing strategy given the observed toxicity limit. Specifically, we are interested in answering the question whether alternative dosing strategies can be applied to circumvent the toxicity limit while exceeding the level of efficacy observed in continuous dosing of lapatinib while taking into account known characteristics of GBM growth and treatment response such as diffusivity, intratumor heterogeneity, and the blood brain barrier.

Materials and methods

Cell culture

SF268 cells were obtained from the National Cancer Institute (NIH) and routinely grown in DMEM supplemented with 10% fetal bovine serum. To assess the effects of drug treatment, 150,000 cells were seeded on 6-cm dishes and allowed to attach overnight. Cells were then switched to growth media supplemented with 1% fetal bovine serum and the indicated concentrations of lapatinib or DMSO (vehicle). Each treatment condition was done in triplicate. For treatment discontinuation, cells were washed 3 times with media containing vehicle, and then allowed to continue growth in media containing vehicle. Vehicle-treated cells were also washed 3 times to control for the effects of washing. Cell viability and cell death were evaluated by the trypan blue exclusion assay using a ViCell cell viability analyzer (Beckman Coulter).

Mathematical modeling

***In vitro* cell dynamics.** To describe *in vitro* cell dynamics, we designed a differential equation model of cell growth given by

$$\frac{dY_1}{dt} = bY_1\left(1 - \frac{Y_1}{K}\right) - dY_1 \tag{1a}$$

$$\frac{dY_2}{dt} = dY_1 - cY_2 \tag{1b}$$

where Y_1 and Y_2 denote the numbers of viable and dead cells, respectively; the parameters b and d denote the birth and death rates of viable cells; K denotes the carrying capacity of the *in vitro* assay system; and c denotes the clearance rate of dead cells.

Grid search algorithm for estimating model parameters. We implemented a grid search algorithm, given by

$$\underset{b,c,d}{argmin}\{(Y_{1,obs}(t) - Y_1(b,d,c,t))^2 + (Y_{2,obs}(t) - Y_2(b,d,c,t))^2\} \tag{2}$$

which minimizes the squared distance between the observed and predicted cell numbers for each experimental setting in order to estimate model parameters that best recapitulate the experimental results.

Characterizing the relationship between birth and death rates and lapatinib dose. We used an exponential model to describe the relationship between birth and death rates and lapatinib dose given by

$$b(L) = b_0 e^{b_1 L}, \tag{3a}$$

$$d(L) = d_0 e^{d_1 L}, \tag{3b}$$

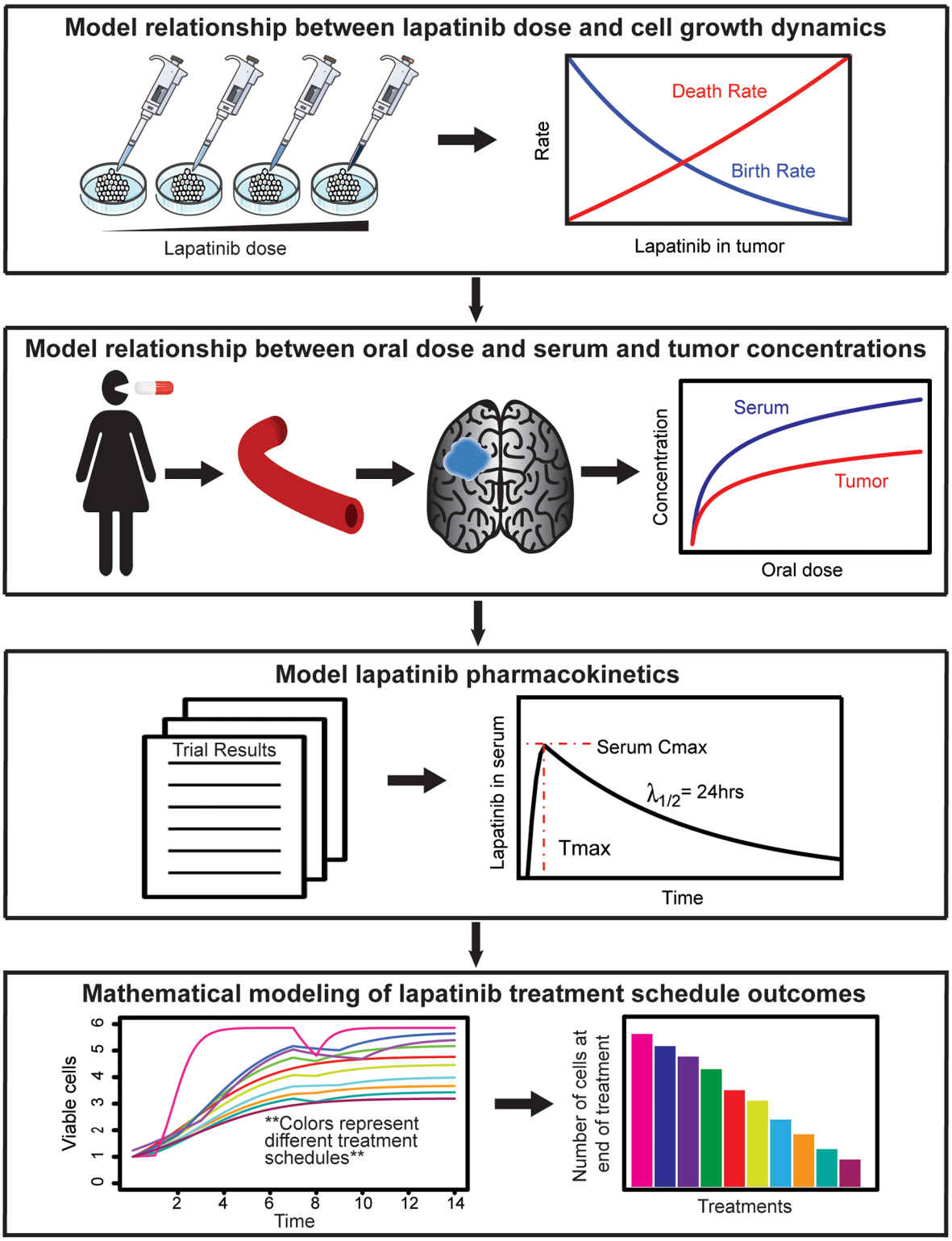

Fig 1. Illustration of the combined experimental and computational modeling approach. First, we establish the relationship between tumor lapatinib concentration and tumor cell dynamics; second, we identify the relationship between oral lapatinib dose, serum lapatinib concentration, and tumor lapatinib concentration; third, we ascertain the pharmacokinetics model describing lapatinib uptake and decay; lastly, we build a mathematical model to compare the efficacies of different lapatinib treatment schedules.

https://doi.org/10.1371/journal.pcbi.1005924.g001

where b_0 and b_1 are the intercept and slope parameters, respectively, describing the birth rate, and d_0 and d_1 are the intercept and slope parameters, respectively, describing the death rate.

Patient-derived toxicity constraints. To characterize the relationship between the maximally tolerated lapatinib dose per treatment and number of treatment days, we fit a linear model given by

$$y_{dose} = \alpha_0 + \alpha_1 x_{days} \tag{4}$$

and an exponential model given by

$$y_{dose} = e^{\beta_0 + \beta_1 x_{days}}, \tag{5}$$

where y_{dose} denotes the lapatinib intake per treatment day and x_{days} is the number of treatment days per treatment cycle.

Lapatinib pharmacokinetics. We fit a logarithmic function to model lapatinib absorption into the blood stream, according to

$$y_{serum}(ng/mL) = \tau_0 + \tau_1 log(x_{oral}(mg)), \tag{6}$$

where x_{oral} is the dose of oral lapatinib in miligrams and y_{serum} is the concentration of lapatinib in the serum in ng/mL units.

To convert serum to tumor lapatinib concentration, we used the conversion

$$y_{tumor}(nM) = 0.61 \times y_{serum}(ng/mL) \times \frac{mol}{943.5 \times 10^9 ng} \times \frac{1000mL}{1L} \tag{7}$$

where y_{serum} is the serum concentration in ng/mL, y_{tumor} is the concentration of lapatinib in the tumor, and 0.61 was the mean tumor/serum ratio reported in Vivanco et al. [32].

Modeling *in vivo* GBM growth using a diffusion equation. We used the following diffusion model to simulate *in vivo* GBM growth

$$\frac{\partial c}{\partial t} = D\nabla^2 c + \rho c\left(1 - \frac{c}{\kappa}\right), \tag{8}$$

where $c(x, t)$ is the concentration of cells in $1mm^3$ volume of tissue at position x and time t, D is the diffusion coefficient defining the net rate of migration of tumor cells, ρ is the net proliferation rate of cells per day, κ is the carrying capacity of the tissue, and ∇^2 is the Laplacian.

To model GBM growth during treatment, we scale ρ by the birth and death rates estimated from the *in vitro* lapatinib treatment data such that

$$\rho(L(t)) = \rho_0 \frac{b(L(t)) - d(L(t))}{b(0) - d(0)}, \tag{9}$$

where $\rho_0 = 0.0387$ is the proliferation rate in the absence of treatment [33], $L(t)$ is the concentration of lapatinib in the tumor at time t, $b(0)$ and $d(0)$ are the birth and death rates in the absence of treatment, and $b(L(t))$ and $d(L(t))$ are the birth and death rates during treatment with $L(t)$ concentration of lapatinib. The diffusion model during treatment is then given by

$$\frac{\partial c}{\partial t} = D\nabla^2 c + \rho(L(t))c\left(1 - \frac{c}{\kappa}\right). \tag{10}$$

Lastly, we assumed an isolated system corresponding to a no-flux boundary condition of the

form

$$\frac{\partial c(0,t)}{\partial x} = \frac{\partial c(R,t)}{\partial x} = 0, \quad 0 \le t \le T \tag{11}$$

where T is the simulation time and R is the radius of the computational domain.

Modeling GBM heterogeneity using diffusion equations. We used the following system of diffusion equations to model intratumor heterogeneity due to the presence of drug-sensitive and -resistant cells:

$$\frac{\partial c_S}{\partial t} = D\nabla^2 c_S + \rho(L(t))c_S\left(1 - \frac{c_R + c_S}{\kappa}\right), \tag{12a}$$

$$\frac{\partial c_R}{\partial t} = D\nabla^2 c_R + \rho_0 c_R\left(1 - \frac{c_R + c_S}{\kappa}\right), \tag{12b}$$

where c_S and c_R represent the concentration of sensitive and resistant cells at position x and time t. The proliferation rate in Eq (12b) given by ρ_0, the proliferation rate in the absence of treatment, because the resistant cells are assumed to be unaffected by treatment.

Modeling reduced lapatinib delivery to the brain. To model reduced lapatinib delivery to the brain due to the blood brain barrier or other reasons, we used a modified diffusion model given by

$$\frac{\partial c}{\partial t} = D\nabla^2 c + \rho(Q * L(t))c\left(1 - \frac{c}{\kappa}\right), \tag{13}$$

where Q denotes the percent of the serum concentration of lapatinib that reaches the tumor.

Modeling the Go-or-Grow mechanism. It is well known that glioblastoma is highly hypoxic, and that one mechanism used by tumor cells to survive in hypoxic environments is a phenotypic switch from proliferative to migratory phenotypes [34], also known as the "Go-or-Grow" mechanism. This phenotypic switch depends on the oxygen concentration in the microenvironment, which we modeled using the following system of three PDEs describing migratory cell, proliferative cell, and oxygen concentration, repectively [35]:

$$\frac{\partial c_M}{\partial t} = D\nabla^2 c_M - f_{MP}(\sigma)c_M + f_{PM}(\sigma)c_P, \tag{14a}$$

$$\frac{\partial c_P}{\partial t} = \rho(L(t))c_P\left(1 - \frac{c_M + c_P}{\kappa}\right) + f_{MP}(\sigma)c_M - f_{PM}(\sigma)c_P, \tag{14b}$$

where $c_M(x, t)$ and $c_P(x, t)$ represent the concentration of migratory and proliferative tumor cells, respectively, at position x and time t, and $\sigma(x, t)$ is the oxygen concentration at position x and time t. The latter is given by the diffusion equation

$$\frac{\partial \sigma}{\partial t} = D_\sigma \nabla^2 \sigma + h_1 \nu(\sigma_0 - \sigma) - h_2(c_M + c_P)\sigma, \tag{15}$$

where D_σ is the oxygen diffusion coefficient, h_1 is the transvasculature permeability, h_2 is the rate at which glioma cells consume oxygen, and σ_0 is the oxygen concentration in normal brain cells. Lastly, $f_{MP}(\sigma)$ and $f_{PM}(\sigma)$ represent the rates at which tumor cells switch from migratory to proliferative and proliferative to migratory phenotypes, respectively. Assuming the rates of switching have a linear dependence on oxygen concentration, the two functions

are then given by

$$f_{MP}(\sigma) = \lambda_2 \sigma, \tag{16a}$$

$$f_{PM}(\sigma) = \lambda_1 - \sigma, \tag{16b}$$

where λ_1 and λ_2 are positive constants.

Testing the relationship between cell motility and treatment response. To test whether the relationship between the cell motility predicted by the diffusion equation and the tumor volume depends on the treatment schedule, we used a linear regression model with interaction terms:

$$V_S = v_0 + v_D D + v_S S + v_{int,S} D * S = (v_0 + v_S * S) + (v_D + v_{int,S} S) D. \tag{17}$$

Here D is the diffusion parameter, S is a categorical variable representing the treatment schedule used, and V_S is the volume at the end of treatment with treatment schedule S. Then, $(v_D + v_{int,\,S}\,S)$ is the slope representing the effect of motility on the tumor volume at the end of treatment, and $v_{int,\,S}\,S$ is the effect of the interaction between cell motility and the treatment schedule. We used schedule 1 as the baseline schedule, meaning that $v_S = v_{int,\,S} = 0$. Thus we can test H_0: $v_{int,\,S} = 0$ to assess whether tumor growth under schedule S is more or less affected by increased cell motility than schedule 1, for S = schedule 2, schedule 3, schedule 4, or schedule 5.

Simulating a clinical trial of treatment schedules. A cohort of $N = 50$ patients was used to simulate each clinical trial to test for differences between treatment schedules. Cell dynamics and pharmacokinetics parameters were randomly sampled for each patient. The same 50 patients were used to evaluate survival outcomes for different treatment schedules. Cell birth and death rate parameters, b_0, b_1, d_0, and d_1, were sampled from $Normal(\hat{\mu}, \hat{\sigma})$ distributions, where $\hat{\mu}$, and $\hat{\sigma}$ are the estimated parameters and corresponding standard errors listed in Table 2. Lapatinib concentration absorption from the serum into the tumor was sampled from a $Beta(2.3, 1.5)$ distribution, which has mean 0.61, the average tumor/serum concentration reported in [32].

In silico trials that additionally varied cell motility sampled the diffusion parameter from a $Gamma(1, 1)$ distribution that was truncated below 0.55 and above 4.23, the diffusion parameter thresholds reported in Murray, 2012 [36]. Diffusion parameter values were then divided by 30 to convert from mm^2/month to mm^2/day.

Table 2. Estimated pharmacodynamic and pharmacokinetic parameters.

Parameter	Estimate	Standard Error	p-value
b_0	1.4153	0.115	9.286×10^{-8}
b_1	-0.001043	1.392×10^{-4}	1.204×10^{-5}
d_0	0.02159	0.0055	0.00237
d_1	8.418×10^{-4}	9.816×10^{-5}	3.351×10^{-6}
α_0	9.02464	0.06392	0.00451
α_1	-0.20599	0.02021	0.06227
β_0	7596.2	632.0	0.0528
β_1	-942.3	199.9	0.1330
τ_0	-2.1987	1.1334	0.0843
τ_1	0.4959	0.1541	0.0105

https://doi.org/10.1371/journal.pcbi.1005924.t002

Results

In vitro tumor cell pharmacodynamics

We first modeled the *in vitro* cell pharmacodynamics during lapatinib treatment using a logistic ordinary differential equation (ODE) model (Eq 1). The choice of a logistic model over simpler exponential models was made based on exploratory analysis of viable cell dynamics over time (Fig 2A and 2B). During treatment with low concentrations of lapatinib, the growth rate of cells leveled off after 5 days; this change in the growth rate as a function of the cell number is better captured by a logistic than an exponential model. Note that the birth, death, and clearance rates and carrying capacity are restricted to be non-negative real numbers. The carrying capacity, K, is assumed to be invariant to lapatinib concentrations and is estimated as the maximum observed number of viable cells on day 5 in the absence of lapatinib. The birth, death, and clearance rate parameters b, d, and c, respectively, are functions of the lapatinib concentration; however, the exact functional form describing the relationship between these rates and the lapatinib dose is unknown.

To estimate the birth, death, and clearance rates that best capture cell growth patterns, we implemented a grid search algorithm (Eq 2) to minimize the squared distance between observed and predicted cell numbers for each experimental setting in order to determine the parameters that best reproduce observed cell numbers. The patterns of birth, death, and clearance rates against lapatinib concentration are shown in S1A–S1C Fig. We observed that, when allowing the clearance rates to vary for different concentrations of lapatinib, only the death rates show a discernible pattern with increasing lapatinib dose (S1B Fig). However, if the clearance rate is constrained to a constant, we observed that both birth and death rates demonstrated clear dose-dependent correlations (S1D–S1F Fig). We thus adopted the latter approach, leading to birth rates exponentially decreasing and death rates exponentially increasing with escalating lapatinib concentrations. To further investigate the effects of a constant clearance rate, we studied a wide range of values for the clearance rate (0.0, 0.1, 0.2, 0.3, 0.4, and 0.5), and found only minor differences in the birth and death rates estimated for different clearance rates. We therefore selected the simplest assumption with a clearance rate of 0, which reduces the final model to Eq (1), with $c = 0$ in Eq (1b).

We then modeled the relationship between birth and death rates and lapatinib dose as exponential distributions (Eq 3). We estimated the distribution coefficients for birth and death rates using nonlinear least squares regression, which are shown in Table 2. We found that birth and death rates are both significantly associated with lapatinib dose ($p_{birth} = 1.204 \times 10^{-5}$, $p_{death} = 3.351 \times 10^{-6}$).

Once we established the relationship between the birth and death rates and the lapatinib concentration, we modeled the growth trajectory for different lapatinib concentrations over time (Fig 2C and 2D) using the model described in Eq 1. We found that the number of viable cells predicted by our model agrees with the observed numbers of viable cells on day 5 (Fig 2E). The model also predicts a clear negative correlation between the lapatinib concentration and the number of viable cells at day 5; however, our model agrees less well with the observed number of dead cells on day 5 (Fig 2F). One possible reason for the discrepancy is that the number of observed dead cells in much smaller than the number of observed viable cells, and hence birth and death rates were determined predominantly using the observed viable cells. Note that our approach does not capture the peak in the number of dead cells on day 3; we believe that this peak does not represent true underlying biology but rather represents a technical artifact since, if we were to include the peak in our analysis, we would estimate growth and death rates that are inconsistent with the know action of anti-cancer agents (i.e. increasing

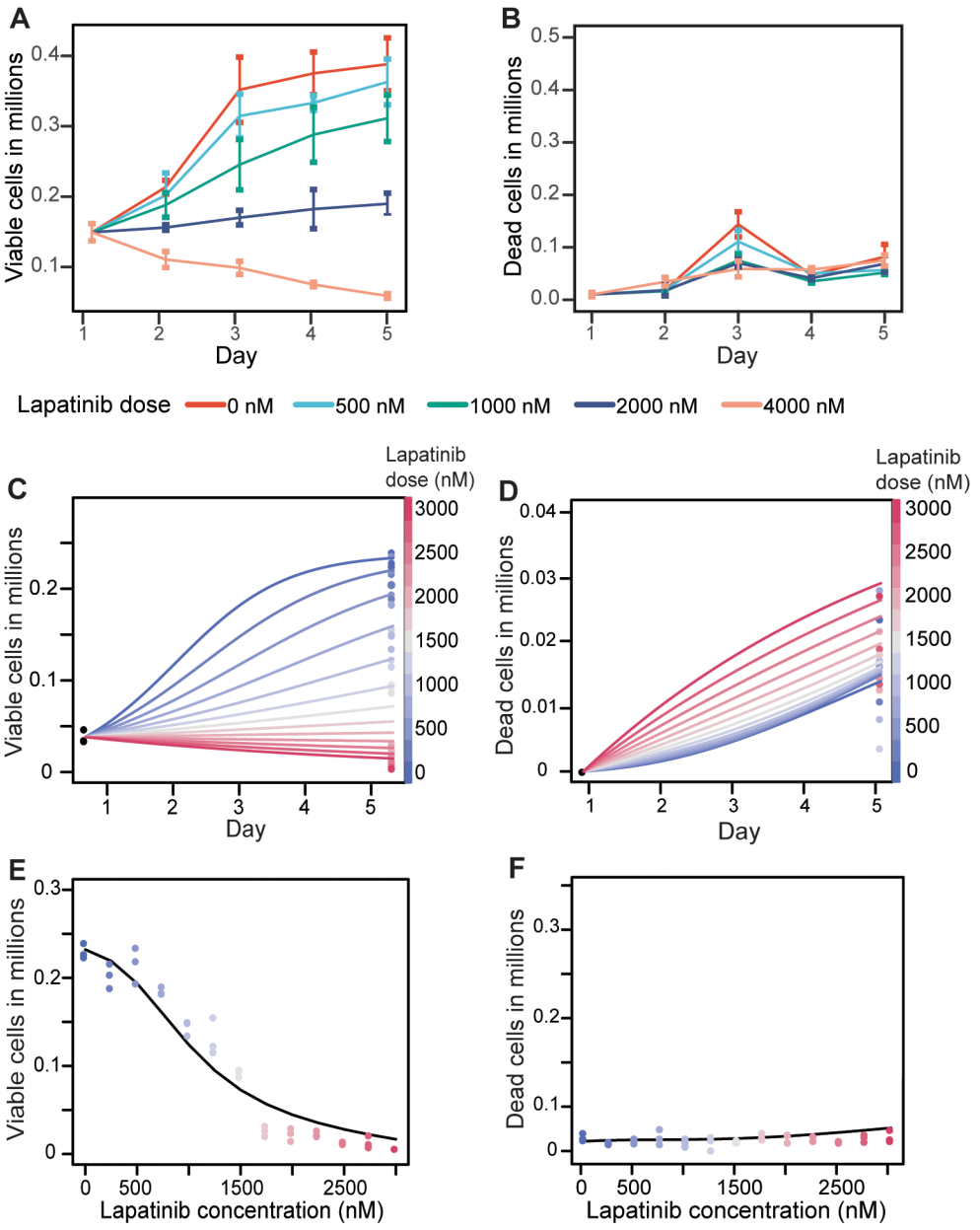

Fig 2. Observed and model-predicted numbers of viable and dead cells over time for varying concentrations of lapatinib. A: The observed number of viable cells over a 5 day period in the presence of varying lapatinib concentrations. B: The observed number of dead cells over a 5 day period in the presence of varying lapatinib concentrations. C: The viable cell trajectories for different concentrations of lapatinib based on the logistic ODE model, where different colored lines represent the model-predicted viable cell growth trajectories for different lapatinib concentrations. D: The dead cell trajectories for different concentrations of lapatinib based on the logistic ODE model, assuming a clearance rate of zero. E-F: Comparisons between model-predicted and observed numbers of viable and dead cells.

https://doi.org/10.1371/journal.pcbi.1005924.g002

doses lead to lower proliferation and/or enhanced death). Designing a model to capture this peak would likely lead to overfitting and hence decreased predictive abilities. For these reasons we decided to use the approach outlined above to describe the cell growth trajectories in the presence of lapatinib treatment.

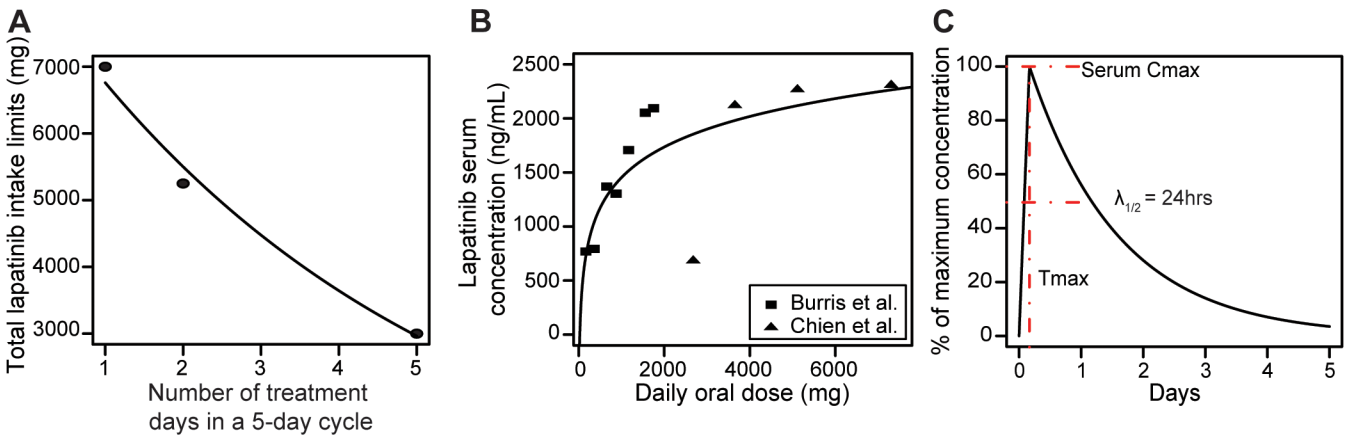

Fig 3. Maximum tolerated dose per treatment cycle and lapatinib pharmacokinetics. A: Maximally tolerated oral lapatinib dose as a function of the numbers of treatment days in a 5-day treatment cycle. The exponential function shown in black is estimated based on the three data points. B: The relationship between oral doses and maximum serum lapatinib concentrations at Cmax, 4 hours after oral intake. A logarithmic function is fitted to estimate the relationship between oral doses and serum concentrations. C: The lapatinib pharmacokinetic profile for modeling serum clearance is determined as a linear-exponential function with C_{max} = 4 hours and $T_{1/2}$ = 24 hours.

https://doi.org/10.1371/journal.pcbi.1005924.g003

Patient-derived toxicity constraints

To identify optimum treatment schedules for the delivery of lapatinib to patients, our approach needs to take into account clinically determined toxicity constraints—the maximally tolerated dose (MTD) for a particular time interval that does not lead to dose-limiting side effects. The maximum allowable oral dose as a function of the number of treated days was constructed from two clinical studies: Thiessen et al. [16] and Chien et al. [17]; a third point was selected based on clinical expertise in order to estimate the shape of this function (Fig 3A). The three toxicity limits we then fitted to both a linear (Eq 4) and an exponential (Eq 5) model (Table 2). We found that the exponential model better explains the observed limiting toxicity as a function of the number of treatment days (AIC values: linear 49.48 vs. exponential 5.712). Limiting doses were extrapolated based on the exponential model for 1 to 5 treatment days in a 5-day treatment cycle.

In vivo lapatinib pharmacokinetics

In addition to modeling tumor cell dynamics in the presence of lapatinib treatment, our approach also requires a model of lapatinib pharmacokinetics—the dynamics of lapatinib absorption into the blood stream, absorption into the tumor, and clearance from the tumor. We first modeled lapatinib absorption into the blood stream using pharmacokinetic parameters from clinical trials (Table 4 in Burris et al [37] and Table 4B in Chien et al. [17]). We then fit a logarithmic function (Eq 6) to this data to describe the relationship between the limiting oral doses identified above to the maximum plasma concentration (Fig 3B, Table 2).

To convert the plasma concentration to tumor concentration, we used patient pharmacokinetic data reported in Table S4 in Vivanco et al. [32]. In this study, the authors found the mean tumor/serum concentration to be 0.61 in biopsied GBMs following 1 week of daily lapatinib treatment. The resulting serum to tumor conversion function is described in Eq 7.

Finally, we constructed a time-dependent pharmacokinetic model using parameters C_{max} = 4 hours, i.e. the time to reach the maximum serum concentration after drug administration, and $T_{1/2}$ = 24 hours, i.e. the time to reach half of the maximum concentration after C_{max} [38].

Table 3. Lapatinib concentrations for MTD treatment schedules.

Schedule	Treatment Days	Oral (mg)	Serum (ng/mL)	In tumor (nM)
1	5	3000	1972	1275
2	4	3642	2083	1347
3	3	4475	2202	1424
4	2	5250	2294	1483
5	1	7000	2460	1590

https://doi.org/10.1371/journal.pcbi.1005924.t003

A linear function was used to model lapatinib uptake from 0 to 4 hours, and an exponential function was used to model the subsequent decay pattern, with a half-life of 24 hours (Fig 3C).

Optimum dosing strategies for lapatinib treatment

Combining tumor cell dynamics with patient derived lapatinib pharmacokinetics provides the *in vivo* tumor growth trajectory—the basis for comparing different dosing strategies. In particular, we compared five treatment schedules that provide the MTD per day according to the identified toxicity constraints, including one continuous dosing strategy and four pulsatile dosing strategies (Table 3).

Optimum dosing strategies using a logistic ODE growth model. We first investigated the five individual treatment schedules using a logistic ODE growth model (Eq 1), which is the simplest growth model possible under our assumptions. The *in vitro* viable cell trajectories for the five treatment schedules for both short-term response (one 5-day cycle) and long-term response (twenty 5-day cycles) are shown in Fig 4A and 4B. Based on this analysis we observed that none of the five schedules is capable of reducing the total number of viable cells either in the short-term or long-term. In the short-term, all pulsed dosing schedules with large up-front loading doses result in slower viable cell growth than the continuous dose schedule on the initial high dose days. However, once switching to the treatment holidays, viable cell growth in the pulsed schedules outpaces that of the continuous schedule, resulting in a sharp increase in the numbers of viable cells. In the long-term, pulsed schedules result in large fluctuations in the number of viable cells. In contrast, the number of viable cells in the continuous schedule increases smoothly over time. In addition, the number of viable cells in the continuous dosing schedule converges to a limit that is lower than the carrying capacity whereas the maximum numbers of viable cells in the four pulsatile dosing schedules are higher than that in the continuous dosing schedule. Finally, comparing the number of viable cells at the end of treatment to a control schedule (no treatment), we see that the continuous dosing schedule results in a 60% reduction in the total number of viable cells at the end of treatment compared to no treatment, whereas the best pulsatile treatment has less than a 30% reduction (Fig 4C). Although lapatinib fails to arrest further tumor expansion, our data suggest that lapatinib has the ability to reduce overall tumor burden below the carrying capacity under a continuous dosing schedule (schedule 1). Additionally, continuous dosing of lapatinib decreases the number of viable cells at the end of 20 treatment cycles compared to the pulsatile treatment schedules.

Optimum dosing strategies using a diffusion PDE growth model. Human GBM is known to be highly diffusive and infiltrative [33, 36, 39–45]. Hence our logistic ODE growth model based on *in vitro* growth may not accurately reproduce some of the important characteristics of human disease as it does not account for tumor cell diffusivity and heterogeneity. In order to better scale our model to human disease, we performed additional analyses using a logistic growth diffusion model (Eq 8). Diffusion models have been widely used to model tumor growth [33, 36, 46–49]; for example, in Swanson et al. [33] the authors showed that they

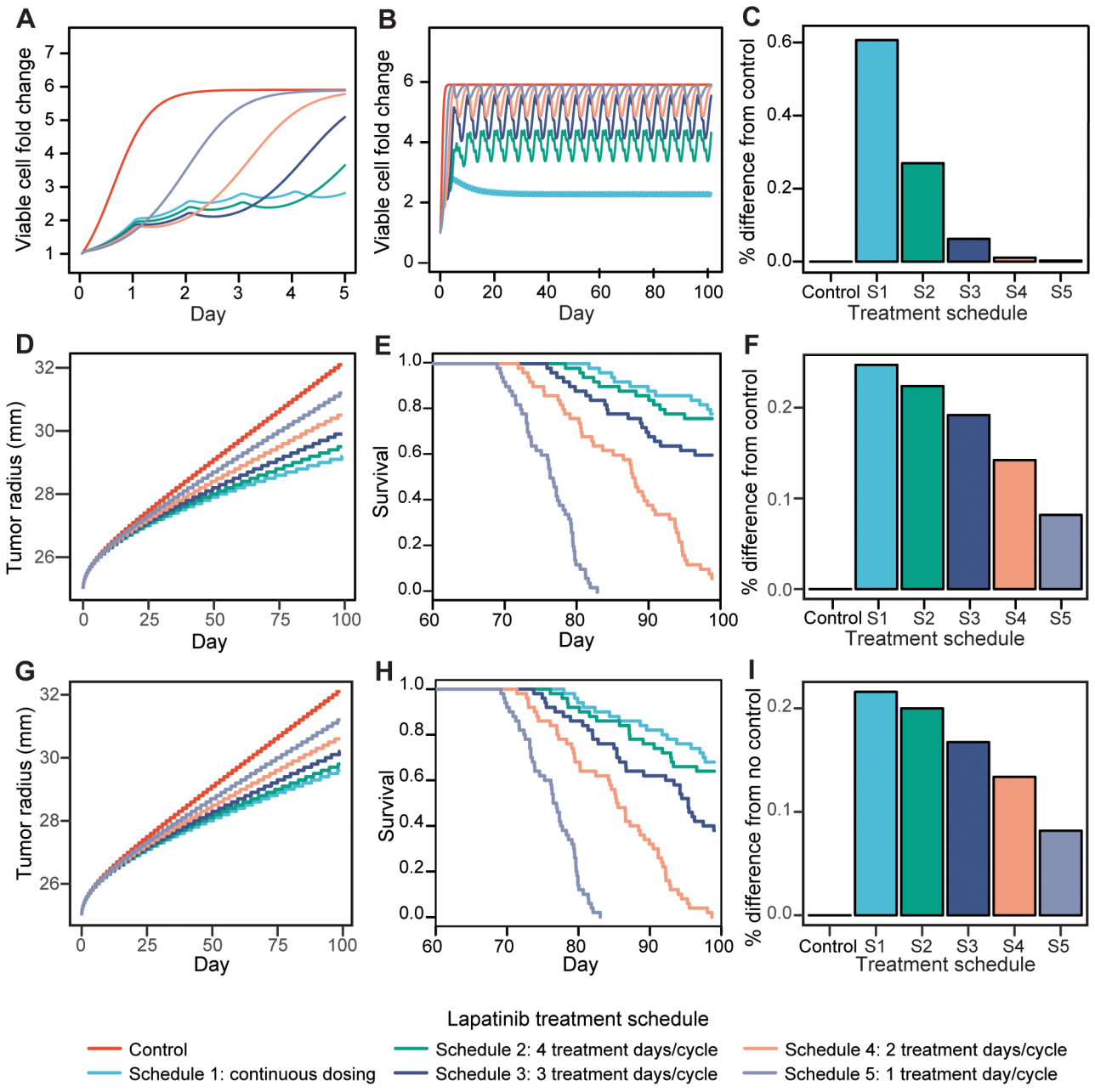

Fig 4. Model-predicted tumor growth trajectories and survival outcomes for five different maximally tolerated dose schedules. A: Predicted short-term tumor growth trajectories for the five MTD treatment schedules (1 treatment cycle) based on the logistic ODE growth model. B: Predicted long-term tumor growth trajectories (20 treatment cycles) for the five MTD treatment schedules based on the logistic ODE model. C: Comparison of the outcomes of the five MTD treatment schedules to the control schedule (no treatment) based on the logistic ODE growth model. The best dosing schedule (smallest tumor volume predicted after 20 treatment cycles) has the highest bar while the control schedule has zero height. D: Predicted long-term tumor growth trajectories (20 treatment cycles) for the five MTD treatment schedules based on the logistic diffusion PDE model. E: Kaplan Meier analysis showing the results of a simulated clinical trial of the five MTD schedules based on the logistic diffusion PDE model. 50 patients were sampled from varying growth rate and PK parameters (see Methods). F: Comparison of the outcomes of the five MTD schedules to the control schedule (no treatment) using the logistic diffusion PDE model. The best dosing schedule (smallest tumor volume predicted after 20 treatment cycles) has the highest bar while the control schedule has zero height. G: Predicted long-term tumor growth trajectories (20 treatment cycles) for the five fixed total dose treatment schedules based on the logistic diffusion PDE model. H: Kaplan Meier analysis showing the results of a simulated clinical trial of the five fixed total dose treatment schedules using the logistic diffusion PDE model. 50 patients were sampled from varying growth rate and PK parameters (see Methods). I: Comparison of the outcomes of the five fixed total dose schedules to the control schedule (no treatment) using the logistic diffusion PDE model. The best dose (smallest tumor volume predicted after 20 treatment cycles) has the highest bar while the control schedule has zero height.

https://doi.org/10.1371/journal.pcbi.1005924.g004

can accurately predict patient survival using a diffusion model for tumor growth, supporting the applicability of such a model for investigating human GBM growth kinetics.

To incorporate the diffusion model into our approach, we used a proliferation rate of ρ = 0.387/day and diffusion parameter $D = 0.03\text{mm}^2/day$, which represent the patient-derived median proliferation and diffusion rates reported in Murray, 2012 [36]. We let the initial solid and isolated cell tumor radii be 1.5cm and 2.5cm, respectively, where the solid and isolated cell tumor volumes represent tumor cell concentrations of 80% and 16%, respectively, of the maximum cell concentration; 1.5cm was the initial solid tumor radius used in [33], and 2.5cm is in the isolated cell radius range reported in Swanson et al. [33]. Note that we chose 2.5cm rather than the median reported isolated cell radius of 2.84cm to allow simulated tumors sufficient time to grow before reaching a radius of 3cm, which is consistently considered to be the "fatal" radius [33]. Finally, we let the lower threshold for detection of cancer cells on an MRI be 8,000 cells/mm^3, and the carrying capacity, κ, be 10^6 cells/mm^3. To model GBM proliferation during treatment, we scaled the proliferation rate by the birth and death rates during treatment estimated from the *in vitro* data (Eq 9). The resulting diffusion model in the presence of treatment is described in Eq 10.

The long-term tumor growth trajectories for the five MTD treatment schedules are shown in Fig 4D. Consistent with our analysis based on the ODE model, we observed that even when using the PDE model, none of the treatment schedules are able to reduce the total tumor volume. However, as before, the continuous dosing schedule again results in slower tumor growth and a reduced tumor volume at the end of treatment compared to the pulsatile dosing strategies (Fig 4F).

Next, we simulated a clinical trial testing the five MTD treatment schedules in a cohort of 50 patients. We varied the GBM growth rates and pharmacokinetic parameters across patients (see Methods) and considered the time of death of a patient to be when their tumor reached 3cm in diameter [33]. The resulting Kaplan-Meier survival distributions are shown in Fig 4E. We observed that patients treated with the continuous dosing schedule (schedule 1) have the best survival outcomes, while patients treated with the one treatment day/cycle schedule (schedule 5) have the worst survival outcomes, which is consistent with the predicted growth rate trajectories in Fig 4D. Moreover, using a log-rank test, we found that the differences between the continuous dosing schedule and schedules 3, 4, and 5 are significant ($p_{schedule3}$ = 0.0316, $p_{schedule4} = 7.7 \times 10^{-16}$, $p_{schedule5} < 2 \times 10^{-16}$). The difference between continuous dosing and schedule 2 (4 treatment days/cycle) is not significant, which is not surprising because the two schedules are very similar.

We observe that the median survival times predicted by our model (80-90 days for schedules 4 and 5) may underestimate survival times observed in the clinic (12-14 months with agressive treatment). However, our analysis suggests that schedules 4 and 5 are only slightly better than no treatment at all. Thus our results are not unreasonable given that median survival for patients receiving no treatment or only palliative antitumor therapy is 8.8 weeks [50], so we are comfortable using this analysis to compare treatment schedules.

By using the MTD on each treatment day for the individual schedules, the total dose administered during a treatment cycle is different for each schedule because administering more frequent treatments of smaller allotments allows administration of more total dose during a treatment cycle compared to less frequent administrations of large doses. The rationale for this approach is to maximize the total dose for each schedule design while still remaining under the MTD. Alternatively, to investigate whether the differences in continuous vs pulsatile dosing are due to differences in the total amount of drug administered, we also investigated tumor growth during five treatment schedules with a fixed total dose (Table 4). The long-term growth trajectories for the five fixed total dose treatment schedules are shown in Fig 4G, the Kaplan-

Table 4. Lapatinib concentrations for fixed total dose treatment schedules.

Schedule	Treatment Days	Oral (mg)	Serum (ng/mL)	In tumor (nM)
1	5	1400	1534	1025
2	4	1750	1661	1074
3	3	2330	1826	1881
4	2	5250	2294	1483
5	1	7000	2460	1590

https://doi.org/10.1371/journal.pcbi.1005924.t004

Meier analyses from the simulated clinical trial using the fixed total dose schedules is shown in Fig 4H, and the comparison of tumor volumes at the end of each treatment are shown in Fig 4I. When implementing this approach, we observed that the ranking of schedules with regard to their treatment efficacies is consistent with our previous results using the maximum tolerated administered dose per day. However, the fixed total dose schedules result in larger tumors at the end of treatment compared to the MTD schedules. Therefore we performed the remainder of our analysis using the MTD schedules listed in Table 3 as our goal is to identify the best overall treatment strategy regardless of the total drug dose administered in one treatment cycle.

Incorporating intratumor heterogeneity into lapatinib treatment response models. Human tumors contain a large extent of intratumor heterogeneity [51–65] which represents a major cause of drug resistance [51, 61, 62, 66]. To determine the effects of intratumor heterogeneity on lapatinib treatment response, we considered a two cell-type population of tumor cells containing lapatinib-sensitive and -resistant cells. This scenario is represented by the model described in Eq (12). We again investigated the five MTD treatment schedules for this scenario when considering different levels of pre-existing resistance (i.e. 0%, 1%, 5%, and 10% pre-existing resistant cells at the start of treatment).

The long-term growth trajectories of tumors with varying pre-existing resistance are shown in S2 Fig, and a comparison of tumor volumes at the end of treatment between the five schedules across different levels of pre-existing resistance is shown in Fig 5A. We found that for 0% and 1% pre-existing resistance, continuous dosing leads to better efficacy than any of the pulsatile dosing schedules; however, when there is 5% or 10% pre-existing resistance, the continuous dosing and 4 doses/cycle schedule (schedule 2) perform similarly, though still better than the other pulsatile dosing schedules. These results indicate that the continuous dosing schedule is preferable to pulsatile dosing even in the presence of a resistant cell population, although the difference among the individual treatment schedules becomes smaller at higher levels of pre-existing resistance.

Non-uniform treatment delivery to the brain. A major reason for GBM treatment failure is insufficient drug delivery to the brain. The blood brain barrier prevents most systematically-delivered molecules from being transported into the brain [67]. Indeed, the tumor concentrations of lapatinib in the patient cohort from Vivanco et al. [32] vary considerably, ranging from 70-3826 nM, as do the plasma/tumor ratios, and the blood brain barrier may be one reason causing such variable lapatinib concentration reaching the tumor.

To establish if the blood brain barrier affects lapatinib treatment response, we made the assumption that the blood brain barrier causes less drug to enter the tumor leading to a decreased drug effect. We adapted our diffusion model to account for reduced drug delivery to the brain by introducing a factor Q in the proliferation rate function (Eq 13). We use this model to assess how much a 10%, 25%, and 50% decrease in the lapatinib concentration reaching the tumor from the serum affects our simulated treatment outcomes. The growth trajectories

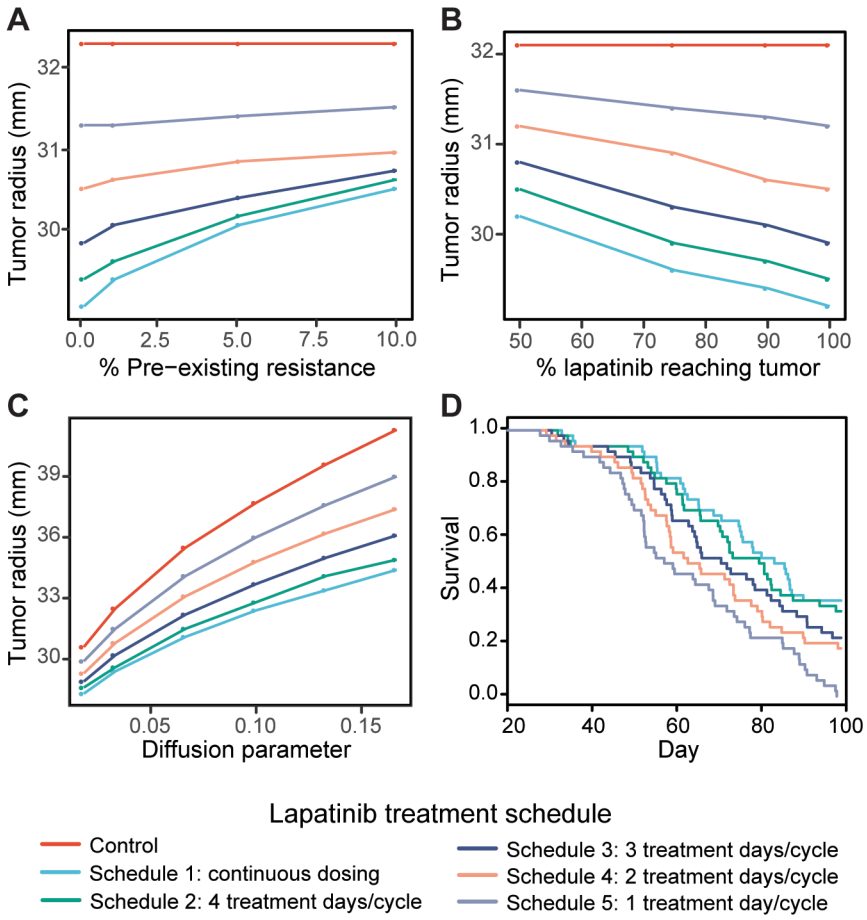

Fig 5. PDE model-predicted effects of intratumor heterogeneity, the blood brain barrier, and differential motility on tumor growth trajectories. A: Comparison of predicted tumor radii at the end of 20 treatment cycles between the five MTD treatment schedules for 0%, 1%, 5%, and 10% pre-existing resistance. B: Comparison of predicted tumor radii at the end of 20 treatment cycles between the five MTD treatment schedules for 50%, 75%, 90%, and 100% of the serum lapatinib concentration entering the tumor. C: Comparison of predicted tumor radii at the end of 20 treatment cycles between the five MTD treatment schedules for diffusion coefficients of 0.0183, 0.033, 0.067, 0.1, 0.133, 0.167 mm^2/day. D: Kaplan Meier analysis showing the survival outcomes of a simulated clinical trial of 50 patients per schedule with variable diffusion parameter.

https://doi.org/10.1371/journal.pcbi.1005924.g005

resulting from different amounts of lapatinib reaching the tumor for each treatment schedule are shown in S3 Fig. We also compared tumor volumes at the end of treatment between treatment schedules across different levels of lapatinib reaching the tumor (Fig 5C). As expected, we observed that decreasing the amount of lapatinib that crosses the blood brain barrier decreases the effect of treatment. However, the decreased effect of treatment is similar across all treatment schedules; hence continuous dosing still remains the best treatment option for reducing long-term tumor growth, even when there is reduced availability of lapatinib in the brain.

The effects of motility on lapatinib treatment response. Tumor cell motility has been described as a source of variability in treatment responses among a patient cohort and measures of motility can be predictive of treatment response [36]. In order to asses the effects of tumor cell motility on treatment outcomes, we simulated tumor growth using Eq (8) for varying values of the diffusion parameter, D, estimated from patient data (ref). For our analyses we utilized D equal to 0.01833, 0.0333, 0.0667, 1.333, and 1.667 mm^2/day, where 0.01833 mm^2/day is the lower limit and 1.667 is above the upper limit reported in Murray, 2012 [36]. Long-

Table 5. Coefficient estimates for the effects of GBM cell motility on tumor growth.

Parameter	Estimate	Standard Error	p-value
v_0	89,410	3,021	$<2 \times 10^{-16}$
v_D	501,579	29,853	2.92×10^{-13}
$v_{schedule2}$	1739	4272	0.6883
$v_{schedule3}$	4162	4272	0.3417
$v_{schedule4}$	7304	4272	0.1028
$v_{schedule5}$	10982	4272	0.0183
$v_{int,\ schedule2}$	43,666	42219	0.3134
$v_{int,\ schedule3}$	138,696	42219	0.0037
$v_{int,\ schedule4}$	258,064	42219	5.66×10^{-6}
$v_{int,\ schedule5}$	411,360	42219	4.89×10^{-9}

https://doi.org/10.1371/journal.pcbi.1005924.t005

term tumor growth for each diffusion parameter is shown in S4 Fig. We additionally compared tumor volumes at the end of treatment between schedules across the diffusion parameters (Fig 5C). Although we found, as expected, that tumors with higher motility grow faster during all treatment schedules, the continuous dosing schedule performs better than all pulsatile dosing strategies across all diffusion parameters tested. We then investigated whether the relationship between motility and tumor volume (in mm^3) at the end of treatment depends on the treatment schedule using linear regression with an interaction term between the diffusion parameter and the schedule (Eq 17). We found that schedules 3, 4, and 5 are significantly more affected by increased motility than schedule 1 (Table 5), indicating that the effectiveness of continuous dosing is less comromised by increased cell motility than that of a pulsatile schedule with only 1, 2, or 3 treatment days per cycle. This observation suggests that a continuous dosing strategy is more effective than pulsatile dosing even with a large extent of cell motility, consistent with our previous results.

Tumor motility heavily depends on the location of the tumor in the brain, as malignant glial cells diffuse more quickly in white matter than gray matter [68], [69]. Thus, tumor motility can be highly variable between patients, depending on where their tumors are located. To further investigate how variability of motility across a patient cohort affects treatment outcomes and survival, we simulated a clinical trial of the five MTD treatment schedules with a varying diffusion parameter in addition to varying cell dynamics and pharmacokinetics parameters (see Methods). The resulting Kaplan Meier analysis is shown in Fig 5D. We observed that patients treated with a continuous dosing schedule have the longest survival, whereas patients treated with schedule 5 have the worst survival outcomes, consistent with our previous results. Using a log-rank test, the difference between the continuous dosing schedule and schedules 4 and 5 are significant ($p_{schedule4} = 0.0104$, $p_{schedule5} = 1.33 \times 10^{-6}$).

Incorporating the Go-or-Grow mechanism into our mathematical framework. Glioblastoma is known to be highly hypoxic [34, 70], and tumor cell invasion is one of many different rescue mechanisms that allow tumors to survive hypoxic conditions [34, 71]. According to the Go-or-Grow hypothesis, in low oxygen conditions, tumor cells undergo a phenotypic switch from proliferative to invasive/migratory phenotypes [72]. Multiple mathematical models have been developed to describe the effects of this phenomenon on tumor growth [35, 73–76]. We adapted Model II described in [35] to investigate the five laptinib treatment schedules under the assumption of the Go-or-Grow model. Our model is decribed in Eqs 14–16 and parameterized using experimentally derived values, as in [35]. We used vascular density $\nu = \frac{1}{2}$; oxygen concentration in normal tissue $\sigma_0 = 2.068 \times 10^{-9}$ mol mm^{-3}; proliferative to migratory

switching parameter $\lambda_1 = 4.134$ nmol mm^{-3} (twice the normal tissue concentration); migratory to proliferative switching paramter $\lambda_2 = 0.5$, 1, and 2; oxygen diffusion rate $D_\sigma = 1.51 \times 10^2$ mm^2 day^{-1}; oxygen supply rate $h_1 = 3.37 \times 10^{-1}$ day^{-1}; and oxygen consumption rate $h_2 = 10^{-2}$ mm cell^{-1} day^{-1} (in the range of values reported in [35]). When implementing this model, we found that continuous dosing performs better than all pulsatile dosing schedules (S5 Fig), consistent with our results above.

Discussion

Here we have presented a computational analysis platform of human GBM growth and treatment response, parameterized using *in vitro* tumor cell data measured based on the SF268 GBM cell line during lapatinib exposure. Our data demonstrate that lapatinib concentrations are negatively correlated with cell birth rates, but positively correlated with death rates. However, the necessary lapatinib concentration needed to arrest further tumor expansion is calculated to be 2,180nM *in vitro*, a concentration that cannot be reached in GBM patients based on current toxicity limits and oral absorption profiles. To achieve this concentration, our absorption model predicts that an oral dose of 34,000mg is required—5 times greater than the highest dose ever tested. The therapeutic potential seems to be restricted by the transport of lapatinib from the gastrointestinal tract to tumor sites. Due to the logarithmic relationship between oral intake and serum concentration, a higher than tolerated dose is required to achieve tumor reduction. Other methods of delivery, such as intravenous injection, may need to be considered to bypass the current delivery problem. This result agrees with the conclusions from early clinical trials that lapatinib failed to reduce tumor sizes [15], [16]. Despite these negative results, our model suggests that continuous lapatinib dosing does have positive effects. Continuous dosing was able to reduce long-term tumor burden significantly more than pulsatile treatment schedules. These findings were consistent with incorporating intratumor heterogeneity due to the presence of drug-resistance cells, variable penetration of the blood brain barrier leading to a reduction of lapatinib concentration in the tumor, and tumor cell motility.

Optimization of dosing strategies for cancer treatments is a complex problem. Our mathematical model provides a quantitative relationship bridging *in vitro* tumor dynamics and *in vivo* lapatinib dose and schedule, taking into account the blood brain barrier, GBM motility, heterogeneity, and phenotypic changes that occur in hypoxic microenvironments. Our approach allows for the systematic comparison between different treatment strategies and their effects on tumor growth. Although none of the tolerable doses and schedules evaluated were found capable of arresting tumor expansion, our approach predicts that continuous treatment within these parameters is likely to be more successful at slowing down tumor growth. Further optimization of effective dosing strategies using our computational platform will benefit from additional dose-limiting toxicity studies that incorporate multiple pulsatile schedules.

Supporting information

S1 Fig. Birth, death and clearance rates for different concentrations of lapatinib. A-C: There is no obvious association between birth and death rates with lapatinib concentrations when clearance rates are allowed to vary. D-F: Constraining the clearance rates to be zero, birth rates decrease with increasing lapatinib concentrations and death rates increase lapatinib concentrations. The solid black lines show the relationships between birth and death rates and lapatinib concentration assuming an exponential function. The exponential function is selected to ensure that birth and death rates are always positive for all concentrations of lapatinib.
(TIF)

S2 Fig. Long-term growth trajectories for variable pre-existing resistance. A-D: Predicted long-term growth trajectories (20 treatment cycles) for the five MTD schedules with 0%, 1%, 5%, and 10% pre-existing resistance based on the logistic diffusion PDE model.
(TIF)

S3 Fig. Long-term growth trajectories for reduced lapatinib penetration of the blood brain barrier. A-D: Predicted long-term growth trajectories (20 treatment cycles) for the five MTD schedules with 50%, 75%, 90%, and 100% of serum lapatinib concentrations penetrating the blood brain barrier and entering into the tumor based on the logistic diffusion PDE model.
(TIF)

S4 Fig. Long-term growth trajectories for variable diffusion parameter. A-D: Predicted long-term growth trajectories (20 treatment cycles) for the five MTD schedules with diffusion parameters equal to 0.0183, 0.033, 0.067, 0.1, 0.133, 0.167 mm^2/day based on the logistic diffusion PDE model.
(TIF)

S5 Fig. Long-term growth trajectories under the Go-or-Grow mechanism. A-C: Predicted long-term growth trajectories (20 treatment cycles) for the control and five MTD schedules with migratory to proliferative switching parameter $\lambda_2 = 0.5, 1, 2$.
(TIF)

Author Contributions

Conceptualization: Igor Vivanco, Franziska Michor.

Data curation: Rui Zhao, Igor Vivanco, Franziska Michor.

Formal analysis: Rui Zhao, Franziska Michor.

Funding acquisition: Franziska Michor.

Investigation: Shayna Stein, Rui Zhao, Hiroshi Haeno, Igor Vivanco, Franziska Michor.

Methodology: Shayna Stein, Rui Zhao, Hiroshi Haeno, Igor Vivanco, Franziska Michor.

Software: Rui Zhao.

Supervision: Franziska Michor.

Writing – original draft: Shayna Stein, Rui Zhao, Franziska Michor.

Writing – review & editing: Shayna Stein, Igor Vivanco, Franziska Michor.

References

1. Wen PY, Kesari S. Malignant Gliomas in Adults. New England Journal of Medicine. 2008; 359(5):492–507. https://doi.org/10.1056/NEJMra0708126 PMID: 18669428
2. Stupp R, Mason WP, van den Bent MJ, Weller M, Fisher B, Taphoorn MJB, et al. Radiotherapy plus Concomitant and Adjuvant Temozolomide for Glioblastoma. New England Journal of Medicine. 2005; 352(10):987–996. https://doi.org/10.1056/NEJMoa043330 PMID: 15758009
3. Das Thakur M, Salangsang F, Landman AS, Sellers WR, Pryer NK, Levesque MP, et al. Modelling vemurafenib resistance in melanoma reveals a strategy to forestall drug resistance. Nature. 2013; 494 (7436):251–255. https://doi.org/10.1038/nature11814 PMID: 23302800
4. Shah NP, Kantarjian HM, Kim DW, Réa D, Dorlhiac-Llacer PE, Milone JH, et al. Intermittent target inhibition with dasatinib 100 mg once daily preserves efficacy and improves tolerability in imatinib-resistant and -intolerant chronic-phase chronic myeloid leukemia. Journal of clinical oncology: official journal of the American Society of Clinical Oncology. 2008; 26(19):3204–12. https://doi.org/10.1200/JCO.2007.14.9260

5. Higa GM, Abraham J. Lapatinib in the treatment of breast cancer. Expert Review of Anticancer Therapy. 2007; 7(9):1183–1192. https://doi.org/10.1586/14737140.7.9.1183 PMID: 17892419
6. Lheureux S, Krieger S, Weber B, Pautier P, Fabbro M, Selle F, et al. Expected Benefits of Topotecan Combined With Lapatinib in Recurrent Ovarian Cancer According to Biological Profile. International Journal of Gynecological Cancer. 2012; p. 1.
7. Garcia AA, Sill MW, Lankes HA, Godwin AK, Mannel RS, Armstrong DK, et al. A phase II evaluation of lapatinib in the treatment of persistent or recurrent epithelial ovarian or primary peritoneal carcinoma: a gynecologic oncology group study. Gynecologic oncology. 2012; 124(3):569–74.
8. Leslie KK, Sill MW, Lankes HA, Fischer EG, Godwin AK, Gray H, et al. Lapatinib and potential prognostic value of EGFR mutations in a Gynecologic Oncology Group phase II trial of persistent or recurrent endometrial cancer. Gynecologic oncology. 2012; 127(2):345–50. https://doi.org/10.1016/j.ygyno.2012.07.127 PMID: 22885469
9. de Souza JA, Davis DW, Zhang Y, Khattri A, Seiwert TY, Aktolga S, et al. A phase II study of lapatinib in recurrent/metastatic squamous cell carcinoma of the head and neck. Clinical cancer research: an official journal of the American Association for Cancer Research. 2012; 18(8):2336–43. https://doi.org/10.1158/1078-0432.CCR-11-2825
10. Del Campo JM, Hitt R, Sebastian P, Carracedo C, Lokanatha D, Bourhis J, et al. Effects of lapatinib monotherapy: results of a randomised phase II study in therapy-naive patients with locally advanced squamous cell carcinoma of the head and neck. British journal of cancer. 2011; 105(5):618–27. https://doi.org/10.1038/bjc.2011.237 PMID: 21829197
11. Sridhar SS, Hotte SJ, Chin JL, Hudes GR, Gregg R, Trachtenberg J, et al. A Multicenter Phase Ii Clinical Trial of Lapatinib (gw572016) in Hormonally Untreated Advanced Prostate Cancer. American Journal of Clinical Oncology. 2010; 33(6):609–613. https://doi.org/10.1097/COC.0b013e3181beac33 PMID: 20042973
12. Bekaii-Saab T, Markowitz J, Prescott N, Sadee W, Heerema N, Wei L, et al. A multi-institutional phase II study of the efficacy and tolerability of lapatinib in patients with advanced hepatocellular carcinomas. Clinical cancer research: an official journal of the American Association for Cancer Research. 2009; 15(18):5895–901. https://doi.org/10.1158/1078-0432.CCR-09-0465
13. Ramanathan RK, Belani CP, Singh DA, Tanaka M, Lenz HJ, Yen Y, et al. A phase II study of lapatinib in patients with advanced biliary tree and hepatocellular cancer. Cancer Chemotherapy and Pharmacology. 2009; 64(4):777–783. https://doi.org/10.1007/s00280-009-0927-7 PMID: 19169683
14. Ravaud A, Hawkins R, Gardner JP, von der Maase H, Zantl N, Harper P, et al. Lapatinib versus hormone therapy in patients with advanced renal cell carcinoma: a randomized phase III clinical trial. Journal of clinical oncology: official journal of the American Society of Clinical Oncology. 2008; 26(14):2285–91. https://doi.org/10.1200/JCO.2007.14.5029
15. Reardon DA, Groves MD, Wen PY, Nabors L, Mikkelsen T, Rosenfeld S, et al. A phase I/II trial of pazopanib in combination with lapatinib in adult patients with relapsed malignant glioma. Clinical cancer research: an official journal of the American Association for Cancer Research. 2013; 19(4):900–8. https://doi.org/10.1158/1078-0432.CCR-12-1707
16. Thiessen B, Stewart C, Tsao M, Kamel-Reid S, Schaiquevich P, Mason W, et al. A phase I/II trial of GW572016 (lapatinib) in recurrent glioblastoma multiforme: clinical outcomes, pharmacokinetics and molecular correlation. Cancer Chemotherapy and Pharmacology. 2010; 65(2):353–361. https://doi.org/10.1007/s00280-009-1041-6 PMID: 19499221
17. Chien AJ, Illi JA, Ko AH, Korn WM, Fong L, Chen Lm, et al. A phase I study of a 2-day lapatinib chemosensitization pulse preceding nanoparticle albumin-bound Paclitaxel for advanced solid malignancies. Clinical cancer research: an official journal of the American Association for Cancer Research. 2009; 15(17):5569–75. https://doi.org/10.1158/1078-0432.CCR-09-0522
18. de Vries Schultink AHM, Suleiman AA, Schellens JHM, Beijnen JH, Huitema ADR. Pharmacodynamic modeling of adverse effects of anti-cancer drug treatment. European journal of clinical pharmacology. 2016; 72(6):645–53. https://doi.org/10.1007/s00228-016-2030-4 PMID: 26915815
19. Hansson EK, Ma G, Amantea MA, French J, Milligan PA, Friberg LE, et al. PKPD Modeling of Predictors for Adverse Effects and Overall Survival in Sunitinib-Treated Patients With GIST. CPT: pharmacometrics & systems pharmacology. 2013; 2(12):e85.
20. Keizer RJ, Gupta A, Mac Gillavry MR, Jansen M, Wanders J, Beijnen JH, et al. A model of hypertension and proteinuria in cancer patients treated with the anti-angiogenic drug E7080. Journal of pharmacokinetics and pharmacodynamics. 2010; 37(4):347–63. https://doi.org/10.1007/s10928-010-9164-2 PMID: 20652729
21. Suleiman AA, Frechen S, Scheffler M, Zander T, Nogova L, Kocher M, et al. A Modeling and Simulation Framework for Adverse Events in Erlotinib-Treated Non-Small-Cell Lung Cancer Patients. The AAPS Journal. 2015; 17(6):1483–1491. https://doi.org/10.1208/s12248-015-9815-8 PMID: 26286677

22. Mould DR, Walz AC, Lave T, Gibbs JP, Frame B. Developing Exposure/Response Models for Anticancer Drug Treatment: Special Considerations. CPT: pharmacometrics & systems pharmacology. 2015; 4 (1):e00016.
23. Kogame A, Tagawa Y, Shibata S, Tojo H, Miyamoto M, Tohyama K, et al. Pharmacokinetic and Pharmacodynamic Modeling of Hedgehog Inhibitor TAK-441 for the Inhibition of Gli1 messenger RNA Expression and Antitumor Efficacy in Xenografted Tumor Model Mice. DRUG METABOLISM AND DISPOSITION Drug Metab Dispos. 2013; 41:727–734. https://doi.org/10.1124/dmd.112.049650
24. Bueno L, de Alwis DP, Pitou C, Yingling J, Lahn M, Glatt S, et al. Semi-mechanistic modelling of the tumour growth inhibitory effects of LY2157299, a new type I receptor TGF-β kinase antagonist, in mice. European Journal of Cancer. 2008; 44(1):142–150. https://doi.org/10.1016/j.ejca.2007.10.008 PMID: 18039567
25. Yamazaki S, Skaptason J, Romero D, Lee JH, Zou HY, Christensen JG, et al. Pharmacokinetic-Pharmacodynamic Modeling of Biomarker Response and Tumor Growth Inhibition to an Orally Available cMet Kinase Inhibitor in Human Tumor Xenograft Mouse Models. Drug Metabolism and Disposition. 2008; 36(7):1267–1274. https://doi.org/10.1124/dmd.107.019711 PMID: 18381487
26. Yamazaki S, Vicini P, Shen Z, Zou HY, Lee J, Li Q, et al. Pharmacokinetic/pharmacodynamic modeling of crizotinib for anaplastic lymphoma kinase inhibition and antitumor efficacy in human tumor xenograft mouse models. The Journal of pharmacology and experimental therapeutics. 2012; 340(3):549–57. https://doi.org/10.1124/jpet.111.188870 PMID: 22129595
27. Wong H, Belvin M, Herter S, Hoeflich KP, Murray LJ, Wong L, et al. Pharmacodynamics of 2-[4-[(1E)-1-(hydroxyimino)-2,3-dihydro-1H-inden-5-yl]-3-(pyridine-4-yl)-1H-pyrazol-1-yl]ethan-1-ol (GDC-0879), a potent and selective B-Raf kinase inhibitor: understanding relationships between systemic concentrations, phosphorylated. The Journal of pharmacology and experimental therapeutics. 2009; 329(1):360–7. https://doi.org/10.1124/jpet.108.148189
28. Grommes C, Oxnard GR, Kris MG, Miller VA, Pao W, Holodny AI, et al. Pulsatile high-dose weekly erlotinib for CNS metastases from EGFR mutant non-small cell lung cancer. Neuro-oncology. 2011; 13 (12):1364–9. https://doi.org/10.1093/neuonc/nor121 PMID: 21865399
29. Calmelet C, Prokop A, Mensah J, Mccawley LJ, Crooke PS. Modeling the Cancer Stem Cell Hypothesis. Math Model Nat Phenom. 2010; 5(3):40–62. https://doi.org/10.1051/mmnp/20105304
30. Yu HA, Sima C, Feldman D, Liu LL, Vaitheesvaran B, Cross J, et al. Phase 1 study of twice weekly pulse dose and daily low-dose erlotinib as initial treatment for patients with *EGFR*-mutant lung cancers. Annals of Oncology. 2016; 28(2):mdw556. https://doi.org/10.1093/annonc/mdw556
31. Chmielecki J, Foo J, Oxnard GR, Hutchinson K, Ohashi K, Somwar R, et al. Optimization of dosing for EGFR-mutant non-small cell lung cancer with evolutionary cancer modeling. Science translational medicine. 2011; 3(90):90ra59. https://doi.org/10.1126/scitranslmed.3002356 PMID: 21734175
32. Vivanco I, Robins HI, Rohle D, Campos C, Grommes C, Nghiemphu PL, et al. Differential sensitivity of glioma- versus lung cancer-specific EGFR mutations to EGFR kinase inhibitors. Cancer discovery. 2012; 2(5):458–71. https://doi.org/10.1158/2159-8290.CD-11-0284 PMID: 22588883
33. Swanson KR, Rostomily RC, Alvord EC. A mathematical modelling tool for predicting survival of individual patients following resection of glioblastoma: a proof of principle. British Journal of Cancer. 2008; 98 (1):113–119. https://doi.org/10.1038/sj.bjc.6604125 PMID: 18059395
34. Jawhari S, Ratinaud MH, Verdier M. Glioblastoma, hypoxia and autophagy: a survival-prone 'ménage-à-trois'. Cell Death and Disease. 2016; 7(10):e2434. https://doi.org/10.1038/cddis.2016.318 PMID: 27787518
35. Alfonso JCL, Köhn-Luque A, Stylianopoulos T, Feuerhake F, Deutsch A, Hatzikirou H. Why one-size-fits-all vaso- modulatory interventions fail to control glioma invasion: in silico insights. Nature Publishing Group. 2016;
36. Murray JD, Murray CJ, Murray J. Journal of Biological Dynamics Glioblastoma brain tumours: estimating the time from brain tumour initiation and resolution of a patient survival anomaly after similar treatment protocols Glioblastoma brain tumours: estimating the time from brain tumour in. Journal of Biological Dynamics. 2012; 6(6):2–118.
37. Burris HA, Taylor CW, Jones SF, Koch KM, Versola MJ, Arya N, et al. A phase I and pharmacokinetic study of oral lapatinib administered once or twice daily in patients with solid malignancies. Clinical cancer research: an official journal of the American Association for Cancer Research. 2009; 15(21):6702–8. https://doi.org/10.1158/1078-0432.CCR-09-0369
38. Paul B, Trovato JA, Thompson J. Lapatinib: a dual tyrosine kinase inhibitor for metastatic breast cancer. American journal of health-system pharmacy: AJHP: official journal of the American Society of Health-System Pharmacists. 2008; 65(18):1703–10. https://doi.org/10.2146/ajhp070646
39. Takano T, Lin JHC, Arcuino G, Gao Q, Yang J, Nedergaard M. Glutamate release promotes growth of malignant gliomas. Nature Medicine. 2001; 7(9):1010–1015. https://doi.org/10.1038/nm0901-1010 PMID: 11533703

40. Quail DF, Joyce JA. The Microenvironmental Landscape of Brain Tumors. Cancer cell. 2017; 31 (3):326–341. https://doi.org/10.1016/j.ccell.2017.02.009 PMID: 28292436

41. Gerstner ER, Chen PJ, Wen PY, Jain RK, Batchelor TT, Sorensen G. Infiltrative patterns of glioblastoma spread detected via diffusion MRI after treatment with cediranib. Neuro-oncology. 2010; 12 (5):466–72. https://doi.org/10.1093/neuonc/nop051 PMID: 20406897

42. Cha J, Kang SG, Kim P. Strategies of Mesenchymal Invasion of Patient-derived Brain Tumors: Microenvironmental Adaptation. Scientific Reports. 2016; 6(1):24912. https://doi.org/10.1038/srep24912 PMID: 27108713

43. Assanah MC, Bruce JN, Suzuki SO, Chen A, Goldman JE, Canoll P. PDGF stimulates the massive expansion of glial progenitors in the neonatal forebrain. Glia. 2009; 57(16):1835–1847. https://doi.org/10.1002/glia.20895 PMID: 19533602

44. Charles NA, Holland EC, Gilbertson R, Glass R, Kettenmann H. The brain tumor microenvironment. Glia. 2011; 59(8):1169–1180. https://doi.org/10.1002/glia.21136 PMID: 21446047

45. Markovic DS, Glass R, Synowitz M, van Rooijen N, Kettenmann H. Microglia stimulate the invasiveness of glioma cells by increasing the activity of metalloprotease-2. Journal of neuropathology and experimental neurology. 2005; 64(9):754–62. https://doi.org/10.1097/01.jnen.0000178445.33972.a9 PMID: 16141784

46. Tracqui P, Cruywagen GC, Woodward DE, Bartoo GT, Murray JD, Alvord EC. A mathematical model of glioma growth: the effect of chemotherapy on spatio-temporal growth. Cell Proliferation. 1995; 28 (1):17–31. https://doi.org/10.1111/j.1365-2184.1995.tb00036.x PMID: 7833383

47. Baldock AL, Rockne RC, Boone AD, Neal ML, Hawkins-Daarud A, Corwin DM, et al. From Patient-Specific Mathematical Neuro-Oncology to Precision Medicine. Frontiers in Oncology. 2013; 3:62. https://doi.org/10.3389/fonc.2013.00062 PMID: 23565501

48. Massey SC, Rockne RC, Hawkins-Daarud A, Gallaher J, Anderson ARA, Canoll P, et al. Simulating PDGF-Driven Glioma Growth and Invasion in an Anatomically Accurate Brain Domain. Bulletin of Mathematical Biology. 2017; p. 1–18.

49. Jackson PR, Juliano J, Hawkins-Daarud A, Rockne RC, Swanson KR. Patient-specific mathematical neuro-oncology: using a simple proliferation and invasion tumor model to inform clinical practice. Bulletin of mathematical biology. 2015; 77(5):846–56. https://doi.org/10.1007/s11538-015-0067-7 PMID: 25795318

50. Coffey RJ, Lunsford LD, Taylor FH. Survival after stereotactic biopsy of malignant gliomas. Neurosurgery. 1988; 22(3):465–73.

51. McGranahan N, Swanton C. Clonal Heterogeneity and Tumor Evolution: Past, Present, and the Future. Cell. 2017; 168(4):613–628. https://doi.org/10.1016/j.cell.2017.01.018 PMID: 28187284

52. Soeda A, Hara A, Kunisada T, Yoshimura Si, Iwama T, Park DM. The Evidence of Glioblastoma Heterogeneity. Scientific Reports. 2015; 5(1):7979. https://doi.org/10.1038/srep07979 PMID: 25623281

53. Burrell RA, McGranahan N, Bartek J, Swanton C. The causes and consequences of genetic heterogeneity in cancer evolution. Nature. 2013; 501(7467):338–345. https://doi.org/10.1038/nature12625 PMID: 24048066

54. Prasetyanti PR, Medema JP. Intra-tumor heterogeneity from a cancer stem cell perspective. Molecular Cancer. 2017; 16(1):41. https://doi.org/10.1186/s12943-017-0600-4 PMID: 28209166

55. Swanton C. Intratumor heterogeneity: evolution through space and time. Cancer research. 2012; 72 (19):4875–82. https://doi.org/10.1158/0008-5472.CAN-12-2217 PMID: 23002210

56. Michor F, Polyak K. The origins and implications of intratumor heterogeneity. Cancer prevention research (Philadelphia, Pa). 2010; 3(11):1361–4. https://doi.org/10.1158/1940-6207.CAPR-10-0234

57. Gerashchenko TS, Denisov EV, Litviakov NV, Zavyalova MV, Vtorushin SV, Tsyganov MM, et al. Intratumor heterogeneity: Nature and biological significance. Biochemistry (Moscow). 2013; 78(11):1201–1215. https://doi.org/10.1134/S0006297913110011

58. Sievers CK, Leystra AA, Clipson L, Dove WF, Halberg RB. Understanding Intratumoral Heterogeneity: Lessons from the Analysis of At-Risk Tissue and Premalignant Lesions in the Colon. Cancer prevention research (Philadelphia, Pa). 2016; 9(8):638–41. https://doi.org/10.1158/1940-6207.CAPR-16-0096

59. Gerlinger M, Rowan AJ, Horswell S, Larkin J, Endesfelder D, Gronroos E, et al. Intratumor Heterogeneity and Branched Evolution Revealed by Multiregion Sequencing. New England Journal of Medicine. 2012; 366(10):883–892. https://doi.org/10.1056/NEJMoa1113205 PMID: 22397650

60. Gay L, Baker AM, Graham TA. Tumour Cell Heterogeneity. F1000Research. 2016; 5. https://doi.org/10.12688/f1000research.7210.1 PMID: 26973786

61. Fisher R, Pusztai L, Swanton C. Cancer heterogeneity: implications for targeted therapeutics. British journal of cancer. 2013; 108(3):479–85. https://doi.org/10.1038/bjc.2012.581 PMID: 23299535

62. Dexter DL, Leith JT. Tumor heterogeneity and drug resistance. Journal of clinical oncology: official journal of the American Society of Clinical Oncology. 1986; 4(2):244–57. https://doi.org/10.1200/JCO.1986.4.2.244

63. Marte B. Tumour heterogeneity. Nature. 2013; 501(7467):327–327. https://doi.org/10.1038/501327a PMID: 24048064

64. Rosenthal R, McGranahan N, Herrero J, Swanton C. Deciphering Genetic Intratumor Heterogeneity and Its Impact on Cancer Evolution. Annual Review of Cancer Biology. 2017; 1(1):223–240. https://doi.org/10.1146/annurev-cancerbio-042516-011348

65. Marusyk A, Almendro V, Polyak K. Intra-tumour heterogeneity: a looking glass for cancer? Nature Reviews Cancer. 2012; 12(5):323–334. PMID: 22513401

66. Schmidt F, Efferth T. Tumor Heterogeneity, Single-Cell Sequencing, and Drug Resistance. Pharmaceuticals (Basel, Switzerland). 2016; 9(2).

67. Zhou J, Atsina KB, Himes BT, Strohbehn GW, Saltzman WM. Novel delivery strategies for glioblastoma. Cancer journal (Sudbury, Mass). 2012; 18(1):89–99.

68. Chicoine MR, Silbergeld DL. Assessment of brain tumor cell motility *in vivo* and *in vitro*. Journal of Neurosurgery. 1995; 82(4):615–622. https://doi.org/10.3171/jns.1995.82.4.0615 PMID: 7897524

69. Kelly PJ, Hunt C. The limited value of cytoreductive surgery in elderly patients with malignant gliomas. Neurosurgery. 1994; 34(1):62–6; discussion 66–7. https://doi.org/10.1097/00006123-199401000-00009 PMID: 8121570

70. Huang WJ, Chen WW, Zhang X. Glioblastoma multiforme: Effect of hypoxia and hypoxia inducible factors on therapeutic approaches. Oncology letters. 2016; 12(4):2283–2288. https://doi.org/10.3892/ol.2016.4952 PMID: 27698790

71. Joseph JV, Conroy S, Pavlov K, Sontakke P, Tomar T, Eggens-Meijer E, et al. Hypoxia enhances migration and invasion in glioblastoma by promoting a mesenchymal shift mediated by the HIF1α-ZEB1 axis. Cancer letters. 2015; 359(1):107–16. https://doi.org/10.1016/j.canlet.2015.01.010 PMID: 25592037

72. Xie Q, Mittal S, Berens ME. Targeting adaptive glioblastoma: an overview of proliferation and invasion. Neuro-oncology. 2014; 16(12):1575–84. https://doi.org/10.1093/neuonc/nou147 PMID: 25082799

73. Alfonso JCL, Talkenberger K, Seifert M, Klink B, Hawkins-Daarud A, Swanson KR, et al. The biology and mathematical modelling of glioma invasion: a review. Journal of the Royal Society, Interface. 2017; 14(136):20170490. https://doi.org/10.1098/rsif.2017.0490 PMID: 29118112

74. Giese A, Loo MA, Tran N, Haskett D, Coons SW, Berens ME. Dichotomy of astrocytoma migration and proliferation. International Journal of Cancer. 1996; 67(2):275–282. https://doi.org/10.1002/(SICI)1097-0215(19960717)67:2<275::AID-IJC20>3.0.CO;2-9 PMID: 8760599

75. Hatzikirou H, Basanta D, Simon M, Schaller K, Deutsch A. 'Go or Grow': the key to the emergence of invasion in tumour progression? Mathematical Medicine and Biology. 2012; 29(1):49–65. https://doi.org/10.1093/imammb/dqq011 PMID: 20610469

76. Gerlee P, Nelander S. The Impact of Phenotypic Switching on Glioblastoma Growth and Invasion. PLoS Computational Biology. 2012; 8(6):e1002556. https://doi.org/10.1371/journal.pcbi.1002556 PMID: 22719241

77. Rich JN, Reardon DA, Peery T, Dowell JM, Quinn JA, Penne KL, et al. Phase II trial of gefitinib in recurrent glioblastoma. Journal of clinical oncology: official journal of the American Society of Clinical Oncology. 2004; 22(1):133–42. https://doi.org/10.1200/JCO.2004.08.110

78. Prados MD, Lamborn KR, Chang S, Burton E, Butowski N, Malec M, et al. Phase 1 study of erlotinib HCl alone and combined with temozolomide in patients with stable or recurrent malignant glioma. Neuro-oncology. 2006; 8(1):67–78. https://doi.org/10.1215/S1522851705000451 PMID: 16443950

79. Brown PD, Krishnan S, Sarkaria JN, Wu W, Jaeckle KA, Uhm JH, et al. Phase I/II trial of erlotinib and temozolomide with radiation therapy in the treatment of newly diagnosed glioblastoma multiforme: North Central Cancer Treatment Group Study N0177. Journal of clinical oncology: official journal of the American Society of Clinical Oncology. 2008; 26(34):5603–9. https://doi.org/10.1200/JCO.2008.18.0612

80. Reardon DA, Egorin MJ, Quinn JA, Rich JN, Rich JN, Gururangan S, et al. Phase II study of imatinib mesylate plus hydroxyurea in adults with recurrent glioblastoma multiforme. Journal of clinical oncology: official journal of the American Society of Clinical Oncology. 2005; 23(36):9359–68. https://doi.org/10.1200/JCO.2005.03.2185

81. Wen PY, Yung WKA, Lamborn KR, Dahia PL, Wang Y, Peng B, et al. Phase I/II study of imatinib mesylate for recurrent malignant gliomas: North American Brain Tumor Consortium Study 99-08. Clinical cancer research: an official journal of the American Association for Cancer Research. 2006; 12(16):4899–907. https://doi.org/10.1158/1078-0432.CCR-06-0773

82. Raymond E, Brandes AA, Dittrich C, Fumoleau P, Coudert B, Clement PMJ, et al. Phase II study of imatinib in patients with recurrent gliomas of various histologies: a European Organisation for Research and Treatment of Cancer Brain Tumor Group Study. Journal of clinical oncology: official journal of the American Society of Clinical Oncology. 2008; 26(28):4659–65. https://doi.org/10.1200/JCO.2008.16.9235